HINGELESS ROTOR FREQUENCY RESPONSE WITH UNSTEADY INFLOW

David A. Peters
Research Scientist
Ames Directorate
U.S. Army Air Mobility R&D Laboratory
Moffett Field, Calif. 94035

Abstract

Hingeless rotor frequency response calculations are obtained by applying a generalized harmonic balance to the elastic blade flapping equations. Nonuniform, unsteady induced flow effects are included by assuming a simple three-degree-of-freedom description of the rotor wake. Results obtained by using various models of elastic blade bending and induced flow are compared with experimental data obtained from a 7.5-ft diameter wind tunnel model at advance ratios from 0.0 to 0.6. It is shown that the blade elasticity and nonuniform, unsteady induced flow can have a significant effect on the transient response characteristics of rotor systems. Good correlation between theory and experiment is obtained by using: (i) a single rotating mode shape description of the elastic blade bending, (ii) an empirical formula for the quasi-steady induced flow behavior, and (iii) the apparent mass terms from potential flow for the unsteady induced flow characteristics.

Notation

a	two-dimensional lift-curve slope, rad^{-1}
a_{jn}, b_{jn}	harmonics of jth flapping mode
b	number of blades
B	tip loss factor
c	blade chord, ft
$\bar{C}_T$	steady value of thrust coefficient, steady thrust/$\rho\pi\Omega^2R^4$
C_T	harmonic perturbation of thrust coefficient
C_L	harmonic perturbation of roll moment coefficient = roll moment/$\rho\pi\Omega^2R^5$, positive advancing blade down
C_M	harmonic perturbation of pitch moment coefficient = pitch moment/$\rho\pi\Omega^2R^5$, positive nose up
e	dimensionless flapping hinge offset
e_{pc}	dimensionless radius of pocket cutout
EI	rotor blade bending stiffness, $lb\text{-}ft^2$
$\{f\}$	generalized response vector
F,G	aerodynamic and inertial forces per unit blade span, lb/ft
g_o, g_s, g_c	nondimensional harmonics of inertial forcing function, Eq. (12)
i	$\sqrt{-1}$
I_A	apparent inertia of air, $slug\text{-}ft^2$
$[I]$	identity matrix
j	index referring to mode number
J	number of flap bending modes
K_m, K_I	nondimensional apparent mass and inertia of impermeable disk
$[K]$	control feedback matrix
$[L]$	nonuniform induced flow matrix
$[L_E]$	empirical value for quasi-steady portion of $[L]$
m	rotor blade mass distribution, slug/ft
$\bar{m}, m_{yy}, m_{yj}$	nondimensional blade parameters $\frac{1}{\rho acR^2}\int_o^R m\,dr$, $\frac{1}{\rho acR^4}\int_o^R mr^2\,dr$, $\frac{1}{\rho acR^3}\int_o^R mr\phi_j\,dr$
$[M], [M']$	rotor response matrix open loop, closed loop
dm	elemental apparent mass, slugs
$\dot{m}$	elemental mass flow, slugs/sec
m_A	apparent mass of air, slugs
n	index referring to harmonic number
N	number of azimuthal harmonics
$[O]$	null matrix
p	first flap frequency divided by Ω
q_j	generalized coordinates
$\bar{q}_j$	steady values of q_j
r	rotor blade radius coordinate, ft
R	rotor blade radius, ft
$S(0,\psi)$	blade root moment, ft-lb
S_j	blade parameter $\frac{1}{\rho acR^2}\int_o^R m\phi_j\,dr$
$\{u\}$	generalized control vector $\langle\theta_o\theta_s\theta_c g_o g_s g_c \lambda_o \lambda_s \lambda_c\rangle$
U_p, U_T	perpendicular, tangential components of air speed in undeformed blade coordinate system, ft/sec
U_∞, V_∞	freestream airspeed perpendicular and parallel to rotor shaft (V_∞ positive down), ft/sec
v	induced flow parameter = $[\mu^2 + \bar{\lambda}(\bar{\lambda} + \bar{\nu})]/(\mu^2 + \bar{\lambda}^2)^{1/2}$
$V(0,\psi)$	blade root shear, lb
w	rotor blade flap deflection, ft
$[W]$	frequency transform, Eq. (23)
$\{x\}$	physical control vector $\langle\theta_o\theta_s\theta_c z\phi\alpha\rangle$
$[Y]$	control coupling matrix
z	hub plunge deflection divided by R, positive down
α	hub pitch angle, positive nose up, rad

Presented at the AHS/NASA-Ames Specialists' Meeting on Rotorcraft Dynamics, February 13-15, 1974.

γ	Lock number, $1/m_{yy}$
γ^*	equivalent Lock number, Eq. (35)
θ	blade pitch angle = $\bar{\theta} + (\theta_o + \theta_s \sin\psi + \theta_c \cos\psi)e^{i\omega\psi}$
$\bar{\theta}$	steady collective pitch angle
$\theta_o, \theta_s, \theta_c$	rotor pitch perturbations
λ	total inflow (including induced flow) $= \bar{\lambda} + \left(\lambda_o + \lambda_s \frac{r}{R} \sin\psi + \lambda_c \frac{r}{R} \cos\psi\right) e^{i\omega\psi}$
$\bar{\lambda}$	steady inflow ratio = $V_\infty/\Omega R + \bar{\nu}$
$\lambda_o, \lambda_s, \lambda_c$	inflow perturbations (including induced flow), Eq. (10)
μ	advance ratio = $U_\infty/\Omega R$
ν	total induced flow = $\bar{\nu} + \left(\nu_o + \nu_s \frac{r}{R} \sin\psi + \nu_c \frac{r}{R} \cos\psi\right) e^{i\omega\psi}$
$\bar{\nu}$	induced flow due to steady rotor thrust
ν_o, ν_s, ν_c	induced flow perturbations
ρ	air density, slug/ft^3
σ	rotor solidity, $bc/\pi R$
τ_T, τ_S	induced flow time constants, rad^{-1}
ϕ	hub roll angle, positive advancing blade down, rad
ϕ_j	orthogonal functions
ψ	rotor blade azimuth position, nondimensional time, rad
ω	excitation frequency divided by Ω
Ω	rotor blade angular velocity, rad/sec
$(\,)'$	$\partial/\partial r$
$(\dot{})$	$\partial/\partial\psi$

The dynamic response characteristics of hingeless rotors are dependent upon the distributed structural properties of the rotor blades, the local aerodynamic properties of the blade sections, and the detailed description of the aerodynamic environment. It is generally believed, however, that reasonable predictions of rotor thrust and moments at low lift can be obtained by using some appropriately simplified models for the blade structure, section aerodynamics, and inflow distribution. The development of these simplified rotor models is useful for gaining insight into the basic dynamic mechanisms of rotor response. Detailed calculations of dynamic airloads, necessary for many applications, are usually too complex for use in basic dynamic research or preliminary design calculations.

The formulation of a minimum complexity rotor response model is the subject of several recent papers. One area of interest is the effect of mode shape and mode number on rotor flapping response. Shupe[1] addresses the effects of the second flap mode, Ormiston and Peters[2] compare various mode shape models for first and second flap modes, and Hohenemser and Yin[3] consider the effect of using rotating rather than nonrotating modes as generalized degrees of freedom. The fundamental conclusion, as clarified in Reference 3, is that for $\mu < 0.8$ a single rotating mode shape is adequate for modeling the steady rotor flapping response.

A second area of interest is the effect of induced flow perturbations on rotor flapping response. In Reference 1, a simple momentum theory predicts a significant effect of induced flow on steady rotor response. In Reference 2, a comparison of steady experimental and theoretical results indicates that, although there is a significant effect due to induced flow, momentum theory is inadequate for predicting this effect in forward flight. Alternate induced flow models are introduced and compared with the data, but no clear choice for the best model is found. In Reference 4, an unsteady momentum theory is used in hover to improve correlations with experimental frequency response data.

The work in References 1 through 4 indicates that a minimum complexity analytic model for rotor dynamics must include appropriate degrees of freedom for both structural and induced flow perturbations (certain flight dynamics programs presently include a simplified dynamic treatment of the induced flow[5]). Unfortunately, while some success has been achieved using simple models of the rotor induced flow in hover, a completely satisfactory induced flow model for forward flight has not been found, not even for the condition of steady response. In addition, neither the physical values of the induced flow time constants nor the frequency range in which they are important is known. The unsteady behavior of the induced flow contributes directly to the low frequency rotor control characteristics and to the coupled rotor/fuselage aeroelastic stability. In particular, induced flow perturbations contribute to the rotor damping available in pitch and roll (which is important for ground and air resonance calculations). It is consequently important to understand the dynamic characteristics of the induced flow.

The purpose of this paper is to provide additional insight into the question of rotor structural and induced flow modeling. To this end, experimental rotor frequency response data in hover and in forward flight are compared with theoretical results that are calculated by using several different models for the elastic blade bending and induced flow. The frequency response data provide a broad base of comparison so that the effects of mode shape and induced flow model can be clearly determined throughout the frequency range of interest.

Basic Equations

Analysis

The mathematical technique used here is a further generalization of the harmonic balance approach of Reference 2. In addition to an arbitrary number of bending modes (with an arbitrary number of azimuthal harmonics for each mode), the generalized harmonic balance allows for a

rational treatment of reversed flow aerodynamics and the possibility of harmonically oscillating control inputs.

The linear equation of motion for the deflection of an elastic beam subject to distributed aerodynamic and inertial loadings $F(r,\psi)$ and $G(r,\psi)$ is[6]

$$(EIw'')'' + m\Omega^2\ddot{w} + \Omega^2\left(mrw' - w''\int_r^R mr\,dr\right) = F(r,\psi) + G(r,\psi) \qquad (1)$$

The associated expressions for bending moment and shear at the blade root are

$$S(0,\psi) = \int_0^R (F + G - m\Omega^2\ddot{w} - m\Omega^2 w)r\,dr \qquad (2)$$

$$V(0,\psi) = \int_0^R (F + G - m\Omega^2\ddot{w})dr \qquad (3)$$

The blade root bending moment is transformed into a stationary coordinate system to yield the pitch and roll moment of the rotor. The solution of Eq. (1) yields directly the blade deflections, and substitution into Eqs. (2) and (3) then yields the forces and moments.

Application of the harmonic balance involves, first of all, an orthogonal expansion of w:

$$\frac{w}{R} = \sum_{j=1}^{J} q_j(\psi)\phi_j(r) \qquad (4)$$

For the present analysis, the ϕ_j are taken to be the exact mode shapes of the rotating beam without aerodynamics. Galerkin's method is then used to transform Eq. (1) into J ordinary differential equations (with periodic coefficients) for the modal coordinates q_j.[6] When the forcing terms contain a steady portion superposed onto periodic functions that are modulated by an excitation frequency ω (cycles per revolution), Floquet's theorem implies that the q_j have a solution of the form[7]

$$q_j = \bar{q}_j + \left\{a_{j0} + \sum_{n=1}^{\infty}\left[a_{jn}\cos(n\psi) + b_{jn}\sin(n\psi)\right]\right\}e^{i\omega\psi} \qquad (5)$$

where $\bar{q}_j$ are the steady coning displacements and the a_{jn} and b_{jn} are complex quantities indicating the magnitude and phase shift of each modulated harmonic of the perturbation response. The harmonic balance approach entails substituting Eq. (5) into the J ordinary differential equations for q_j and setting coefficients of like harmonics equal. When n is truncated at the highest harmonic of interest N, then $(2 \cdot N + 1) \cdot J$ linear algebraic equations are obtained for the a_{jn} and b_{jn}. Solution of these equations, followed by a substitution of Eq. (5) into Eqs. (2) and (3), results in the phase and magnitude of all desired harmonics of the flapping deflections and hub forces and moments.

Blade Loading

The aerodynamic loading of each blade is given by

$$F = \frac{\rho ac}{2}|U_T|\left(U_T\theta - U_P\right) \qquad (6)$$

where

$$U_T = \Omega r + \Omega R\mu\sin\psi \qquad (7)$$

$$U_P = \Omega\dot{w} + \Omega R\lambda + \Omega R\mu w'\cos\psi \qquad (8)$$

Eq. (8) contains the primary contributions of mode shape and induced flow to the flapping equations. The details of blade mode shape become important as μ increases because U_P depends upon both the blade deflection w and its first derivative w'. The induced flow is important because first order perturbations to the inflow λ create first order changes to U_P and F.

Although the inflow is in general a complicated function of radius and azimuth, as a first approximation, the total inflow can be represented by

$$\lambda = \bar{\lambda} + \left[\lambda_o + \lambda_s\frac{r}{R}\sin\psi + \lambda_c\frac{r}{R}\cos\psi\right]e^{i\omega\psi} \qquad (9)$$

The steady portion of the total inflow $\bar{\lambda}$ contains contributions from the freestream velocity $V_\infty/\Omega R$ and from the steady induced flow due to rotor thrust $\bar{\nu}$. The unsteady inflow components $\lambda_o,\lambda_s,\lambda_c$ contain contributions from harmonic plunging $ze^{i\omega\psi}$, rolling $\phi e^{i\omega\psi}$, and pitching $\alpha e^{i\omega\psi}$ of the shaft, as well as contributions from the unsteady induced flow components ν_o,ν_s,ν_c due to perturbations in rotor thrust and moments:

$$\left.\begin{aligned}\lambda_o &= -i\omega z + \nu_o - \mu\alpha\\ \lambda_s &= -i\omega\phi + \nu_s\\ \lambda_c &= -i\omega\alpha + \nu_c\end{aligned}\right\} \qquad (10\ a\text{-}c)$$

The blade pitch angle θ is given by

$$\theta = \bar{\theta} + \left[\theta_o + \theta_s\sin\psi + \theta_c\cos\psi\right]e^{i\omega\psi} \qquad (11)$$

where $\bar{\theta}$ is the steady value of θ and $\theta_o,\theta_s,\theta_c$ are control system perturbations. The inflow perturbations $\lambda_o,\lambda_s,\lambda_c$ are assumed to be

small compared with unity. This implies that the induced flow perturbations ν_o,ν_s,ν_c and the control perturbations $\theta_o,\theta_s,\theta_c,z,\phi,\alpha$ are also small quantities yielding linear perturbation equations.

The inertial loading of each blade is given by

$$G = -m\Omega^2 R\left[g_o + g_s \frac{r}{R}\sin\psi + g_c \frac{r}{R}\cos\psi\right]e^{i\omega\psi} \quad (12)$$

where

$$\left.\begin{aligned} g_o &= \omega^2 z \\ g_s &= \omega^2\phi + 2i\omega\alpha \\ g_c &= -2i\omega\phi + \omega^2\alpha \end{aligned}\right\} \quad (13\ a\text{-}c)$$

The inertial loading is a result of centrifugal, Coriolis, and gyroscopic forces which occur in the rotating reference frame of the blade due to hub motions z,ϕ,α in the inertial reference frame.

When Eqs. (6) through (12) are combined and appropriately integrated in Eqs. (1), (2), and (3), the steady deflections and forces $q_j,\bar{C}_T/\sigma a$ are obtained as linear functions of the steady inputs $\bar{\theta},\bar{\lambda}$; and the perturbation blade deflections and hub forces and moments are obtained as linear combinations of the generalized control variables

$$\langle u\rangle = \langle \theta_o\theta_s\theta_c g_o g_s g_c \lambda_o\lambda_s\lambda_c \rangle \quad (14)$$

Although g_o,g_s,g_c are simply related to the shaft motion through Eq. (13), they are retained as generalized controls so that the generalized controls can be separated into physical, inertial, and aerodynamic groupings. This will facilitate the calculation of rotor response when induced flow is included later.

Interpretation of Results

The results of the harmonic balance can be expressed in matrix form as

$$\{f\} = [M]\{u\} \quad (15)$$

where $\{f\}$ represents the perturbation harmonics of thrust, moments, and generalized coordinates. The elements of $[M]$, therefore, have direct physical significance. They are the partial derivatives of each of the response harmonics taken with respect to each of the generalized controls u_j. The generalized control variables are in turn functions of the physical controls x_j,

$$\langle x\rangle = \langle \theta_o\theta_s\theta_c z\phi\alpha \rangle \quad (16)$$

as evidenced in Eqs. (10) and (13).

The generalized control variables u_j are also coupled to the f_j, because the thrust and moments influence the induced flow. The induced flow, therefore, is a feedback loop of Eq. (15), causing the u_j to depend upon the f_j.

From the standpoint of calculation, it is convenient to express the coupling relation (between the generalized controls, the physical controls, and the rotor response) in matrix form:

$$\{u\} = [Y]\{x\} + [K]\{f\} \quad (17)$$

Eq. (17) is simply a set of linear equations describing: (i) the generalized control perturbations due to application of the physical controls $[Y]$ and (ii) the generalized control perturbations due to the effect that rotor response has on the induced flow $[K]$. The matrices $[Y]$ and $[K]$ will be obtained later by using an appropriate induced flow model. It follows that the partial derivatives of the f_j with respect to the physical controls x_j can be found (including induced flow effects) from Eqs. (15) and (17). The derivative matrix is designated $[M']$ and has the properties

$$\{f\} = [M']\{x\} \quad (18)$$

$$[M'] = \left[[I] - [M][K]\right]^{-1}[M][Y] \quad (19)$$

Although the higher harmonics are often necessary in the harmonic balance calculation of $[M]$, the subsequent calculation of $[M']$ by Eq. (19) may be performed for only those response and inflow harmonics of interest. In this paper, five harmonics are used in the calculation of $[M]$, but only first harmonics are retained in Eqs. (18) and (19), so that the f_j are taken to be

$$\langle f\rangle = \left\langle \frac{C_T}{\sigma a}\ \frac{C_L}{\sigma a}\ \frac{C_M}{\sigma a}\ a_{j0}\ b_{j1}\ a_{j1} \right\rangle \quad (20)$$

Induced Flow

Form of Induced Flow Model

A useful form of the induced flow model is given by[2]

$$\begin{Bmatrix}\nu_o\\ \nu_s\\ \nu_c\end{Bmatrix} = [L]\begin{Bmatrix}C_T/\sigma a\\ C_L/\sigma a\\ C_M/\sigma a\end{Bmatrix} \text{ aerodynamic only} \quad (21)$$

Although not completely general, Eq. (21) can accommodate a variety of induced flow models. Only aerodynamic contributions are included on the right-hand side, because they are the only loads which produce reaction forces on the rotor wake. Using Eqs. (2) and (3), these aerodynamic forces and moments can be expressed in matrix form as

$$\begin{Bmatrix} C_T/\sigma a \\ C_L/\sigma a \\ C_M/\sigma a \end{Bmatrix}_{\substack{\text{aero-}\\ \text{dynamic}}} = \begin{Bmatrix} C_T/\sigma a \\ C_L/\sigma a \\ C_M/\sigma a \end{Bmatrix} + \begin{bmatrix} \bar{m} & 0 & 0 \\ 0 & -\frac{1}{2}m_{yy} & 0 \\ 0 & 0 & -\frac{1}{2}m_{yy} \end{bmatrix} \begin{Bmatrix} g_o \\ g_s \\ g_c \end{Bmatrix}$$

$$- [W] \begin{bmatrix} S_j & 0 & 0 \\ 0 & -\frac{1}{2}m_{yj} & 0 \\ 0 & 0 & -\frac{1}{2}m_{yj} \end{bmatrix} \begin{Bmatrix} a_{jo} \\ b_{j1} \\ a_{j1} \end{Bmatrix} \tag{22}$$

where

$$[W] \equiv \begin{bmatrix} \omega^2 & 0 & 0 \\ 0 & \omega^2 & 2i\omega \\ 0 & -2i\omega & \omega^2 \end{bmatrix} \tag{23}$$

With the induced flow ν described by Eqs. (21) and (22), the inflow relation follows directly from Eqs. (10), (13), and (21). The matrices [Y] and [K] of Eq. (17) may then be identified as

$$[Y] = \begin{bmatrix} I_{3\times3} & 0_{3\times3} \\ 0_{3\times3} & [W]_{3\times3} \\ 0_{3\times3} & [L][W]\begin{bmatrix} \bar{m} & 0 & 0 \\ 0 & -\frac{1}{2}m_{yy} & 0 \\ 0 & 0 & -\frac{1}{2}m_{yy} \end{bmatrix} - \begin{bmatrix} i\omega & 0 & \nu \\ 0 & i\omega & 0 \\ 0 & 0 & i\omega \end{bmatrix} \end{bmatrix} \tag{24}$$

$$[K] = \begin{bmatrix} 0_{3\times3} & 0_{3\times3J} \\ 0_{3\times3} & 0_{3\times3J} \\ [L]_{3\times3} & -[L][W]\begin{bmatrix} S_j & 0 & 0 \\ 0 & -\frac{1}{2}m_{yj} & 0 \\ 0 & 0 & -\frac{1}{2}m_{yj} \end{bmatrix}_{3\times3J} \end{bmatrix} \tag{25}$$

Eq. (24) represents the control coupling between the physical controls x_j and the generalized controls u_j. The presence of [L] in this matrix indicates that the λ's are indirectly coupled (through the induced flow), as well as geometrically coupled [Eqs. (10) and (13)] to the rotor plunge, pitch, and roll motions. Eq. (25) represents the induced flow caused by the dependence of λ upon the thrust and first harmonic flapping. If a suitable approximation to the inflow can be modeled in the form of Eq. (21), then Eqs. (24) and (25) may be substituted directly in Eq. (19) to obtain the complete rotor response to physical control inputs.

Unsteady Momentum Theory

An approximation of the induced flow that is suitable for Eq. (21) can be obtained as an extension of the momentum theory used in Reference 2. The differential force on an elemental area of rotor disk is written as

$$dF = 2\Omega R\nu d\dot{m} + \Omega^2 R\dot{\nu} dm \tag{26}$$

where $2\Omega R\nu$ is the total change in velocity normal to the disk, $d\dot{m}$ is the differential mass flow through the element, dm is the apparent mass associated with the flow, and $\dot{\nu}$ is the time derivative of ν in the nonrotating system. The differential mass flow relation

$$d\dot{m} = \rho\Omega R \sqrt{\mu^2 + \lambda^2}\, r\, dr\, d\psi \tag{27}$$

can be used to integrate the first term of Eq. (26) over the disk to obtain a quasi-steady induced flow relation for rotors that have combined conditions of thrust and forward speed. The evaluation of the second term in Eq. (26) (the unsteady effect) requires the additional knowledge of the apparent mass dm associated with the flow.

An approximation to the apparent mass terms of a lifting rotor can be made in terms of the reaction forces (or moments) on an impermeable disk which is instantaneously accelerated (or rotated) in still air. This approximation was used in Reference 8, giving good agreement with transient thrust measurements for an articulated rotor. The reactions on such an impermeable disk are given from potential flow theory in terms of elliptic integrals which are evaluated in the literature.[9] They result in apparent mass and inertia values

$$m_A = \frac{8}{3}\rho R^3 , \qquad I_A = \frac{16}{45}\rho R^5 \tag{28}$$

(For $\nu = \nu_o\, r/R$, a radial velocity distribution, $m_A = \rho R^3$.) These values represent 64 percent of the mass and 57 percent of the rotary inertia of a sphere of air having radius R. It is emphasized that they are only approximations to the actual values for a lifting rotor.

Using this approximation, the steady induced flow equation and the unsteady induced flow perturbation equations can be derived from Eqs. (26) through (28):

$$2\bar{\nu}\sqrt{\mu^2 + \bar{\lambda}^2} = \bar{C}_T \tag{29a}$$

$$\left.\begin{aligned} K_m\dot{\nu}_o + 2\nu\nu_o &= C_T \\ K_I\dot{\nu}_s + \tfrac{1}{2}\nu\nu_s &= -C_L \\ K_I\dot{\nu}_c + \tfrac{1}{2}\nu\nu_c &= -C_M \end{aligned}\right\} \tag{29b-d}$$

where

$$v \equiv \frac{\mu^2 + \bar{\lambda}(\bar{\lambda} + \bar{\nu})}{\sqrt{\mu^2 + \bar{\lambda}^2}} \tag{29e}$$

and

$$\left.\begin{aligned} K_m &\equiv \frac{m_A}{\rho\pi R^3} = \frac{8}{3\pi} = 0.8488 \\ K_I &\equiv \frac{I_A}{\rho\pi R^5} = \frac{16}{45\pi} = 0.1132 \end{aligned}\right\} \tag{30a-b}$$

Eq. (29a) expresses the nonlinear relation between the steady thrust and the steady induced flow $\bar{\nu}$. Eqs. (29b-d) are then the linear perturbation equations for small changes in thrust, moments, and induced flow. In order for the perturbation equations to be valid, it is assumed that ν_o, ν_s, ν_c are much smaller than $(\mu^2 + \bar{\lambda}^2)^{1/2}$.

The time constants associated with the induced flow model in Eq. (29) are

$$\left.\begin{aligned} \tau_T &= \frac{K_m}{2v} = 0.4244/v \qquad (\text{for } \nu_o) \\ \tau_S &= \frac{2K_I}{v} = 0.2264/v \qquad (\text{for } \nu_s, \nu_c) \end{aligned}\right\} \tag{31a-b}$$

In Reference 4, the steady induced flow $\bar{\nu}$ and the time constant for ν_s, ν_c are obtained by correlating experimental hover frequency response data. Two operating conditions are considered, and the best fit in these cases is found to be $\bar{\nu} = .014$, $\tau_s = 8$ (with $\bar{\theta} = 2°$) and $\bar{\nu} = .028$, $\tau_s = 4$ (with $\bar{\theta} = 8°$). From the $\bar{\nu}$ values indicated for these cases, it can be shown that each τ_s implies the same value of $K_I = 0.112$. Thus, there is some experimental evidence that the potential flow value $K_I = 0.113$ is approximately valid.

By assuming simple harmonic motion, Eqs. (29b-d) can be brought into the form of Eq. (21), yielding the components of [L] for unsteady momentum theory.

$$[L] = \begin{bmatrix} \dfrac{\sigma a}{2v + K_m i\omega} & 0 & 0 \\ 0 & \dfrac{-\sigma a}{v/2 + K_I i\omega} & 0 \\ 0 & 0 & \dfrac{-\sigma a}{v/2 + K_I i\omega} \end{bmatrix} \tag{32}$$

(L_{22} and L_{33} differ by a factor of 4/3 from Reference 2, because ν_s and ν_c are taken uniform with r in that reference, whereas they are taken linear with r here.) The matrix [L] from Eq. (32) may now be substituted into Eqs. (24), (25), and (19) to obtain the rotor response that includes inflow.

Empirical Model

Experimental data have shown that momentum theory, although particularly simple to use, is qualitatively inaccurate for certain steady response derivatives in forward flight.[2] Reference 2 introduces an alternate induced flow model for forward flight in which the elements of [L] (with $\omega = 0$) are chosen to give the best fit of experimental response data for several configurations at conditions of near zero lift. If this empirical inflow model, $[L_E]$, is taken for the quasi-steady portion of the induced flow law, and if the theoretical apparent mass terms (from potential flow) are taken as a model for the unsteady portion of the induced flow law, then a complete induced flow equation can be expressed as

$$\frac{1}{\sigma a}\begin{bmatrix} K_m & 0 & 0 \\ 0 & -K_I & 0 \\ 0 & 0 & -K_I \end{bmatrix}\begin{Bmatrix} \dot{\nu}_o \\ \dot{\nu}_s \\ \dot{\nu}_c \end{Bmatrix} + [L_E]^{-1}\begin{Bmatrix} \nu_o \\ \nu_s \\ \nu_c \end{Bmatrix} = \begin{Bmatrix} C_T/\sigma a \\ C_L/\sigma a \\ C_M/\sigma a \end{Bmatrix} \tag{33}$$

The assumption that the apparent mass terms may be superposed on the quasi-steady terms is not rigorous, but it can be considered analogous to unsteady wing theory in which the apparent mass terms are theoretically independent of the free-stream velocity. Under the superposition assumption, the empirical inflow model modified for the unsteady case is

$$[L] = \left[\begin{bmatrix} K_m & 0 & 0 \\ 0 & -K_I & 0 \\ 0 & 0 & -K_I \end{bmatrix}\frac{i\omega}{\sigma a} + [L_E]^{-1}\right]^{-1} \tag{34}$$

Although this particular formulation of [L] is valuable for predicting the effects of induced flow, ultimately a more consistent formulation of [L] should be made, as discussed in Reference 10.

Equivalent Lock Number

Another method of accounting for the unsteady induced flow is the use of an equivalent Lock number γ^*, which can be derived from a single harmonic balance of the root moment equation:

$$\frac{\gamma^*}{\gamma} = 1 - \frac{1}{1 + 8v/\sigma a + 16K_I i\omega/\sigma a} \tag{35}$$

Although this approach is not a completely consistent treatment of the induced flow, since it does not give an exact harmonic balance of the blade flapping and thrust equations, it yields results which are nearly the same as those obtained from momentum theory.[2]

The practical use of Eq. (35) is somewhat limited because of the inaccuracies of momentum theory in forward flight, but a γ^* approach is nevertheless a valuable conceptual tool for understanding the effects of induced flow. In particular, Eq. (35) shows that one effect of induced flow perturbations is to decrease the effective Lock number (i.e., decrease the aerodynamic effectiveness). This decrease is most pronounced at low values of ν (i.e., low μ and $\bar{\theta}$) and low values of ω. For example, rotor roll moment is plotted in Figure 1 for two values of $\bar{\theta}$ and compared with the value from elementary theory (steady induced flow only, induced flow perturbations neglected, equivalent to $\lim \bar{\theta} \to \infty$). The curves for $\bar{\theta} = 0, 0.05$ result in values of roll moment well below the elementary value.

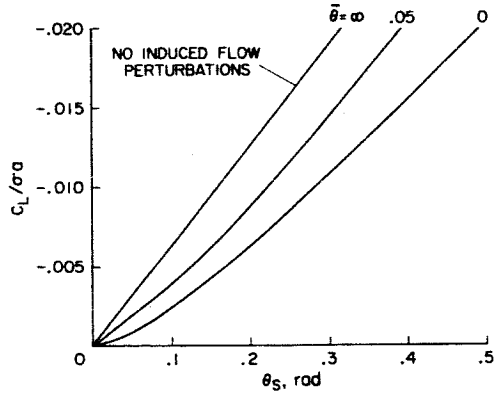

Figure 1. Effect of induced flow on steady rotor response in hover, $\mu = 0$, $\omega = 0$, $\sigma = 0.1$, $a = 2\pi$, $p = \infty$.

The effect of induced flow is most pronounced in the response derivative (the slope of the response curve at $\theta_s = 0$). For $p = \infty$, the derivative is given by

$$\partial\left[C_L/\sigma a\right]/\partial\theta_s\Big|_{\theta_s=0} = -\frac{1}{16}\frac{\gamma^*}{\gamma}\left(1 + 3/2\,\mu^2\right) \quad (36)$$

indicating that $\gamma^*/\gamma < 1$ results in a reduction of the roll moment response (or control power) from the elementary value. When the rotor is in hover with no lift ($\nu = 0$), a quasi-steady perturbation of θ_s ($\omega = 0$) results in no response because of the zero slope of the curve in Figure 1. The mathematical justification for the vanishing response derivative can be seen in Eqs. (35) and (36). With $\omega = \nu = 0$, γ^*/γ and the response derivative must equal zero. As $\bar{\theta}$ increases, however, $\bar{\nu}$ and ν increase so that γ^*/γ approaches unity and the derivative approaches -1/16, as illustrated in Figure 2. Within the practical range of thrust coefficients, however, the response derivative never recovers more than about 80 percent of the elementary value. Eq. (35) also implies that increasing advance ratio (which increases ν) will result in a partial recovery of γ^*/γ (and of the response derivative). This recovery is evident in

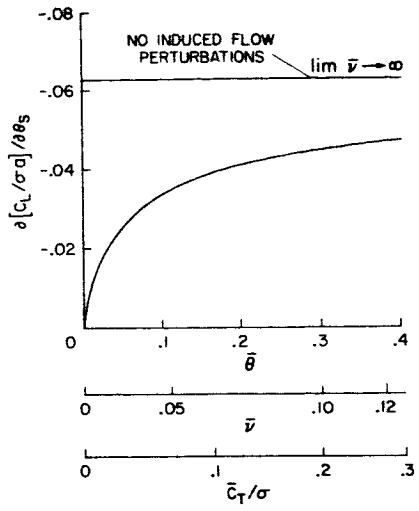

Figure 2. Effect of induced flow on steady rotor response derivatives in hover, $\mu = 0$, $\omega = 0$, $\sigma = 0.1$, $a = 2\pi$, $p = \infty$.

Figure 3, where the roll response is given versus μ; but no more than 90 percent of the elementary value is reached in the practical range of thrust and advance ratio.

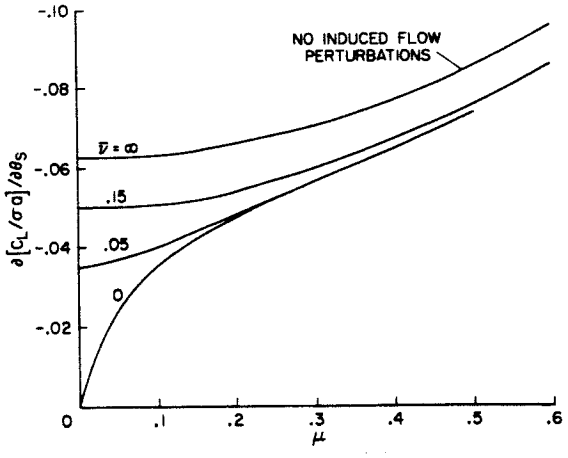

Figure 3. Effect of induced flow on steady rotor response derivatives in forward flight, $\omega = 0$, $\sigma = 0.1$, $a = 2\pi$, $p = \infty$.

The unsteady terms (apparent inertia K_I) also bring γ^*/γ closer to unity, as seen by the role of K_I in Eq. (35). This recovery with frequency is illustrated in Figure 4, where, as ω becomes large, the response derivative approaches the elementary value of -1/16. The rate at which the response approaches -1/16 is dependent upon the magnitude of the apparent inertia K_I. Large values of K_I result in a rapid return to the elementary value, and small values of K_I result in a slow return. For $K_I = 0.1132$ and $\omega < 0.3$, the unsteady terms provide only small contributions to the response. Thus, the quasi-

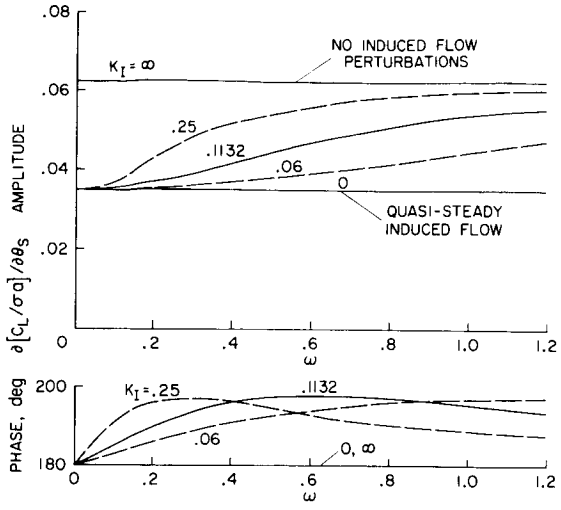

Figure 4. Effect of induced flow time constant on rotor frequency response derivatives, $\mu = 0$, $\sigma = 0.1$, $a = 2\pi$, $p = \infty$, $\bar{\nu} = \bar{\lambda} = 0.05$.

steady theory (with $K_I = 0$) would be adequate in this range. In the frequency range $0.3 < \omega < 1.0$, the unsteady terms have a more significant effect. Above $\omega = 1.2$, the total effect of induced flow diminishes so that the elementary theory and the unsteady theory give similar results; but the quasi-steady theory (with $K_I = 0$) is in considerable error in this region.

The frequency range in which unsteady induced flow is important is also dependent upon the thrust or mean inflow $\bar{\nu}$ as shown in Figure 5. For low values of $\bar{\nu}$, the unsteady effects dominate at low frequencies; and for large values of $\bar{\nu}$, the unsteady effects are delayed into the higher frequencies. This effect is implicit in Eq. (35) and is a direct result of the inverse dependence of time constant upon v, Eq. (31). Thus, a low $\bar{\nu}$ implies a slow induced flow response; and a high $\bar{\nu}$ implies a rapid induced flow response. Equation (35) shows that advance ratio (which also increases v) has a similar effect on the induced flow behavior. It follows that the relative importance of the unsteady and quasi-steady nonuniform induced flow terms depends upon both the rotor operating conditions and the frequency range of interest.

In Figure 6, the relative importance of these terms is presented qualitatively through a chart of the operating regimes in which (for no induced flow or quasi-steady induced flow) $|\gamma^*|$ differs by less than 10 percent from the unsteady value. This is a subjective criterion and is merely intended to illustrate the trends with thrust, advance ratio, and frequency. Four regions are defined: (i) at high ω and v, induced flow effects are small and either the elementary or quasi-steady approximation is adequate; (ii) at high ω and low v, although induced flow effects are small (no induced flow being a good approximation), the quasi-steady

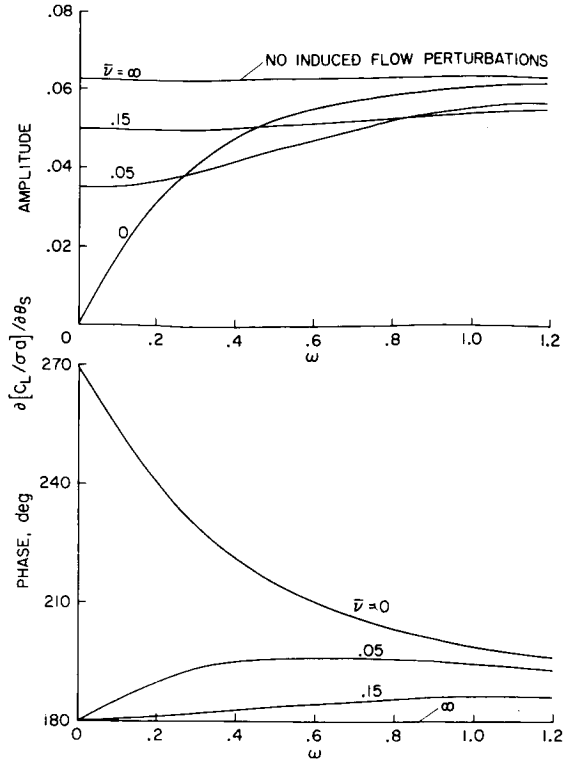

Figure 5. Effect of unsteady induced flow on rotor frequency response derivatives, $\mu = 0$, $\sigma = 0.1$, $a = 2\pi$, $p = \infty$, $K_I = 0.1132$.

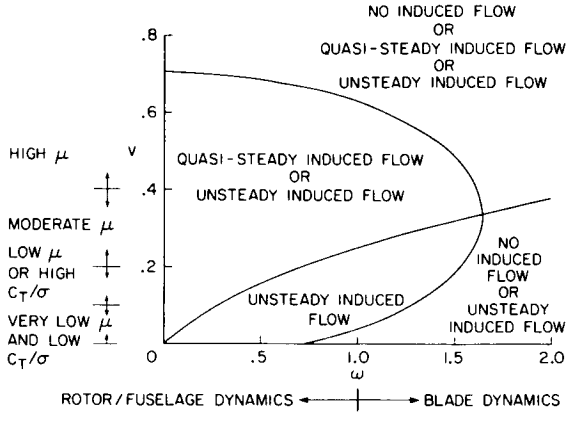

Figure 6. Regions of validity for steady (no induced flow perturbations) quasi-steady ($K_I = K_m = 0$), and unsteady ($K_I = 0.1132$, $K_m = 0.8488$) induced flow models based on γ^*, Eq. (35), $\sigma = 0.1$, $a = 2\pi$.

theory alone will be in error; (iii) at low ω and high v, the opposite is true (i.e., the quasi-steady nonuniform theory is required, whereas neglecting induced flow results in error); and (iv) for low ω and v, complete unsteady theory is required.

Comparison of Theory and Experiment

The experimental data used in the following correlations were obtained with a 7.5-ft-diameter hingeless rotor model tested in the USAAMRDL-Ames wind tunnel.[11] The model configuration and test conditions covered a wide range of parameters. The results included here are for $p = 1.15$ and advance ratios from 0.0 to 0.6.

Elastic Blade Bending

In Fig. 7, experimental values of roll and pitch moments due to θ_s are compared with theoretical results which are calculated neglecting induced flow perturbations. Two sets of theory are presented. The first theory employs a rigid centrally-hinged blade with root spring to model the elastic blade bending, and the second theory uses a similar model, except that hinge offset is allowed. The largest differences between the two theories occur near resonant frequencies, i.e., $\omega = 0.15, 1.15$. (The primary effect of mode shape is aerodynamic, Eq. (8); it causes dominance at resonance.) A surprising element in Figure 7 is that the centrally hinged model gives closer agreement with the high frequency response than does the hinge offset model. This reversal, however, is not a consistent trend in the data and may be somewhat coincidental.

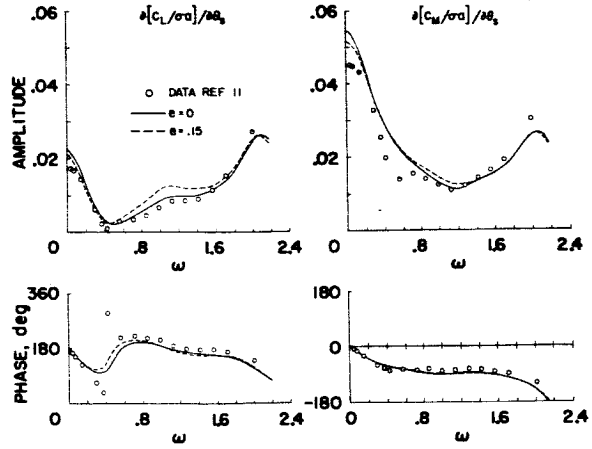

Figure 7. Comparison of experimental data with rigid blade approximations without induced flow, $p = 1.15$, $\gamma = 4.25$, $B = 0.97$, $e_{pc} = 0.25$, $\mu = 0.60$.

Similar frequency response comparisons have been made when the blade is modeled by one or two of the rotating elastic mode shapes. When $\mu < 0.8$ and ω is at least once-per-revolution below the second flap frequency, the one- and two-mode calculations are within a few percent of the hinge-offset results. At higher advance ratios and frequencies, the effects of second-mode bending can become significant; but in the range of operating conditions considered here, a single rotating mode is sufficient to model the blade.

Three major types of discrepancies between theory and experiment which are found in Figure 7 cannot be explained in terms of flapping mode shape effects. The first is the difference encountered at frequencies near one and two per revolution. This difference may be explained by the fact that the lead-lag frequency of this configuration is near two per revolution, causing resonance at these frequencies. The second discrepancy is the irregularity in the pitch response at $\omega = 0.6$. Here, a natural frequency of the rotor support stand is being excited and contaminates the data.[11] The third discrepancy is found at $\omega < 0.6$, and will be shown to result from unsteady inflow perturbations.

Effect of Induced Flow In Hover

The low-frequency hover data provide some insight into the effects of unsteady induced flow. In Figure 8, rotor roll and pitch moments versus θ_s are presented. The experimental results are for $\bar{\theta} = 4°$, $\bar{v} = 0.03$. The theoretical results are calculated using the actual blade rotating mode shape as a generalized coordinate and using three different representations of the induced flow. The first representation is the elementary model, which completely neglects induced flow perturbations. The second representation is quasi-steady momentum theory, which neglects the apparent inertia ($K_I = 0$), assuming that nonuniform induced flow perturbations instantaneously follow the blade dynamics. The third representation is unsteady momentum theory, which gives a time lag on the induced flow perturbations. (The empirical model is not applicable in hover.)

A comparison of theory and experiment reveals that the elementary theory is unsatisfactory below $\omega = 0.6$, failing to reproduce even the qualitative character of the data. On the other hand, the theories which include induced flow perturbations account for most of the important features of the response. The loss of aerodynamic effectiveness, which is a result of induced flow perturbations, causes a decrease in the excitation forces and an overall decrease in the response. But the loss of aerodynamic effectiveness also lowers the blade damping, causing a resonant peak effect near the blade natural frequency (with $p = 1.15$, $\omega = 0.15$).

The effect of the unsteady induced flow terms is also evidenced in Figure 8. The major contribution of K_I is the determination of how rapidly with ω the aerodynamic effectiveness returns to the elementary value. Above $\omega = 0.6$, the theoretical value of K_I gives the proper amplitude and phase for the hub moments, while the quasi-steady theory ($K_I = 0$) fails to return to the conventional value and does not agree with the data. Below $\omega = 0.6$ the comparison is less clear. In the roll-moment phase and amplitude, a K_I less than 0.1132 would give better correlation than does this theoretical value. In the pitch-moment response, however, a smaller K_I would give worse correlation than does $K_I = 0.1132$. Further work would be necessary to determine if this effect is due to experimental difficulties (such as recirculation) or to an actual deficiency in the induced flow model.

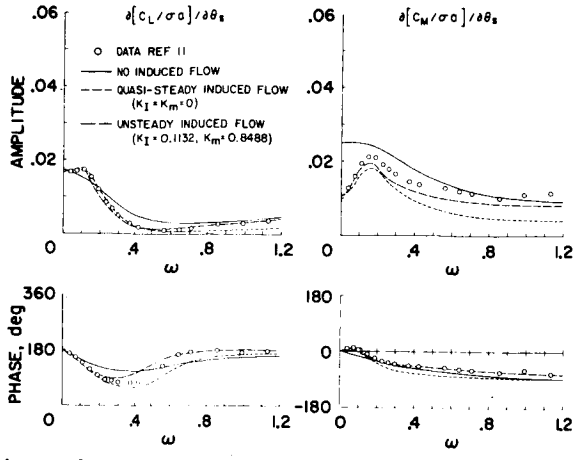

Figure 8. Rotor response to cyclic pitch in hover, $p = 1.15$, $\gamma = 4.25$, $B = 0.97$, $e_{pc} = 0.25$, $\mu = 0$, $\sigma a = 0.7294$, $\bar{v} = \bar{\lambda} = 0.03$, momentum theory, single rotating mode.

In Figure 9, rotor roll and pitch moments versus α are presented for the same test conditions as in Figure 8. Data are presented for shaft excitations in both roll and pitch, since in hover the response to these controls is ideally symmetric. A comparison of the two sets of data gives an indication of the experimental error due to test stand dynamics (and possibly recirculation). Although the data are questionable for $\omega > 0.3$, the lower frequency data substantiate three of the observations made from Figure 8. First, the elementary theory is qualitatively inaccurate for amplitude and phase response. Second, a major effect of induced flow is a resonant peak effect near $\omega = 0.15$. Third, $K_I < 0.1132$ would give better correlation than the theoretical value at low ω. Figure 9 also

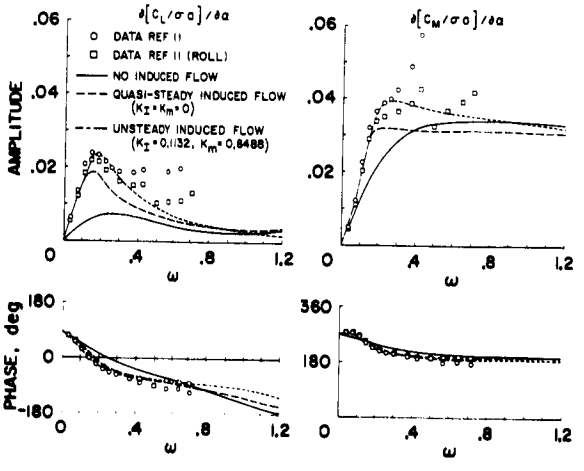

Figure 9. Rotor response to hub motions in hover, $p = 1.15$, $\gamma = 4.25$, $B = 0.97$, $e_{pc} = 0.25$, $\mu = 0$, $\sigma a = 0.7294$, $\bar{v} = \bar{\lambda} = 0.03$, momentum theory, single rotating mode.

shows that although induced flow decreases the blade damping, it can actually increase the rotor pitch/rate damping $= -\mathrm{Re}[\partial(C_M/\sigma a)/\partial\dot{\alpha}]$ and also increase the rotor pitch/roll coupling $= -\mathrm{Re}[\partial(C_L/\sigma a)/\partial\dot{\alpha}]$. The damping and coupling can be found by dividing the plotted curves by $-i\omega$, $\dot{\alpha} = i\omega\alpha$, which is approximately equivalent to taking the slope of the plotted curves with a 90-degree shift in phase angle. For this particular configuration, the damping and coupling are increased by induced flow effects, indicating that induced flow perturbations can be important in coupled rotor/fuselage dynamics.

Effect of Induced Flow in Forward Flight

In the next three figures, experimental data at high-advance ratio ($\mu = 0.51$) and very low lift ($\bar{\theta} \approx 0.5°$) are compared with theory using three induced flow descriptions. The first description is an analysis which neglects induced flow perturbations, the second description is the empirical model of Reference 2 with no time lag (quasi-steady, $K_I = K_m = 0$), and the third description is the empirical model of Reference 2 adapted to the unsteady case according to Eq. (34) (with the

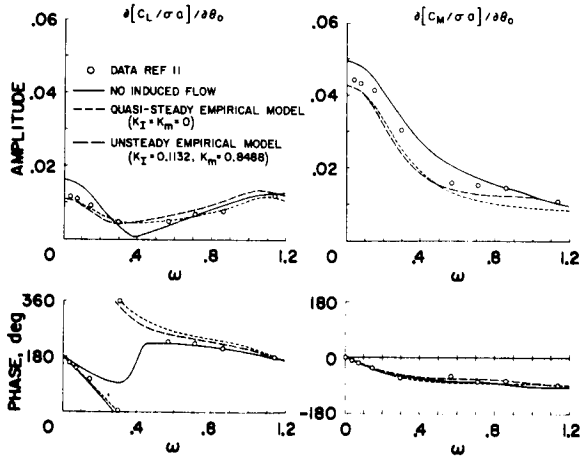

Figure 10. Rotor response to collective pitch in forward flight, $p = 1.15$, $\gamma = 4.25$, $B = 0.97$, $e_{pc} = 0.25$, $\mu = 0.51$, $\sigma a = 0.7294$, $\bar{v} = \bar{\lambda} = 0$, single rotating mode.

theoretical values of K_I and K_m). The first comparison of theory and experiment is shown in Figure 10 for the roll- and pitch-moment response due to θ_o. The elementary theory predicts a roll moment of 0.017 at $\omega = 0$ and a near-zero crossing (amplitude = 0, phase angle discontinuous) at $\omega = 0.4$. The data, however, displays a much lower steady value and completely avoids the zero crossing. The unsteady and quasi-steady empirical models provide a fairly accurate description of this behavior, showing quantitative agreement with phase and magnitude for $\omega < 0.6$. For the pitch moment derivative, the empirical models predict the qualitative (but not the quantitative) aspects of the reduction in moment (from the conventional value) due to induced flow.

Another comparison of theory and experiment is shown in Figure 11 for the roll- and pitch-moment response due to θ_s. The empirical models predict a roll-moment derivative which is less than the elementary value, exhibiting a near-zero crossing at $\omega = 0.26$. This characteristic is clearly evident in the magnitude and phase of the data, but it does not appear in the theory

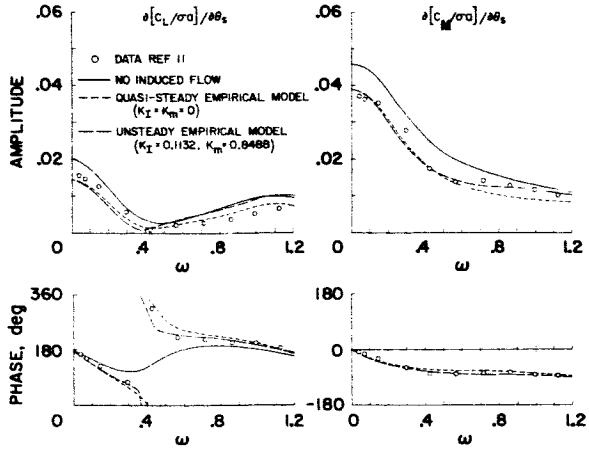

Figure 11. Rotor response to longitudinal cyclic pitch in forward flight, $p = 1.15$, $\gamma = 4.25$, $B = 0.97$, $e_{pc} = 0.25$, $\mu = 0.51$, $\sigma a = 0.7294$, $\bar{\nu} = \bar{\lambda} = 0$, single rotating mode.

without induced flow. For the pitch-moment derivative, the elementary theory agrees with the data only for $\omega > 1.2$; the quasi-steady theory shows good correlation for $0 < \omega < 0.6$, and the unsteady theory gives quantitative correlation at all frequencies.

The third comparison is shown in Figure 12 for the roll- and pitch-moment response due to θ_c. The data show that the roll-moment derivative is less than the elementary value at $\omega = 0$, displaying a resonant peak (near $\omega = 0.15$) which is greater than the elementary value and which is accompanied by a 10-degree phase shift. The empirical models predict the qualitative character of the resonant peak and quantitative character of the phase shift. The empirical models also correlate well with the pitch-moment response, for which the experiment shows the derivative to be greater than the elementary value for $\omega < 0.3$ and less than the elementary value for $\omega > 0.3$.

In general, the empirical inflow models show this same degree of correlation at all advance ratios considered ($\mu = 0.27, 0.36, 0.51, 0.60$). This substantiates one of the qualitative conclusions of Figure 6. For moderate advance ratios and $\omega < 1.0$, an appropriate unsteady or quasi-steady induced flow theory is adequate, but the theory without induced flow is in considerable error. Of course, Figure 6 only implies in which regions quasi-steady or unsteady terms may be significant. It does not imply that any particular quasi-steady or unsteady model will be

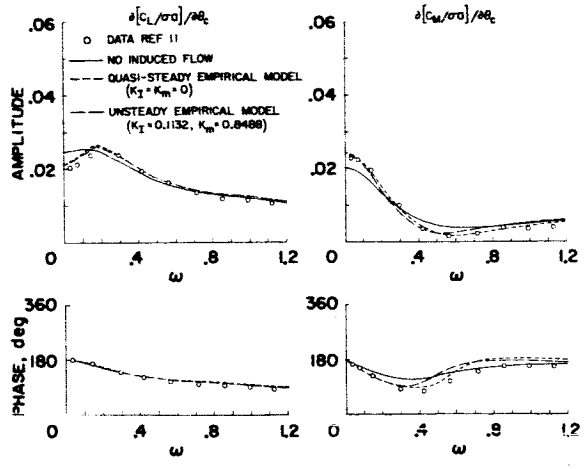

Figure 12. Rotor response to lateral cyclic pitch in forward flight, $p = 1.15$, $\gamma = 4.25$, $B = 0.97$, $e_{pc} = 0.25$, $\mu = 0.51$, $\sigma a = 0.7294$, $\bar{\nu} = \bar{\lambda} = 0$, single rotating mode.

adequate. For example, in Figure 13, pitch moment derivates (as calculated using the theory without induced flow, unsteady momentum theory, and unsteady empirical theory) are compared with the experimental data. The comparison shows that unsteady momentum theory can be in qualitative disagreement with the data even though empirical theory shows good correlation. Even the empirical model, however, does not show complete quantitative correlation; and further refinements in the induced flow model may be necessary.

Conclusions

1. On the basis of an equivalent Lock number relation and $p = \infty$, quasi-steady nonuniform induced flow perturbations can have a significant effect on rotor response throughout the entire thrust/advance ratio range; but the time lag of the induced flow is only important at low lift and low advance ratio.

2. In hover, unsteady momentum theory with apparent mass terms from potential flow provides a significant improvement in data correlation over the theory without induced flow perturbations; but further work is required to refine the induced flow model.

3. In forward flight and near-zero lift, the empirical inflow model of Reference 2, whether used with the unsteady time-lag effect or without the time-lag effect (quasi-steady), correlates well with most qualitative and some quantitative aspects of the data, while unsteady momentum theory and the theory without induced flow provide little agreement with the data.

4. A single rotating mode is sufficient for flapping response calculations when $\mu < 0.8$ and when the major excitation frequency is at least once-per-revolution below the second flapping frequency.

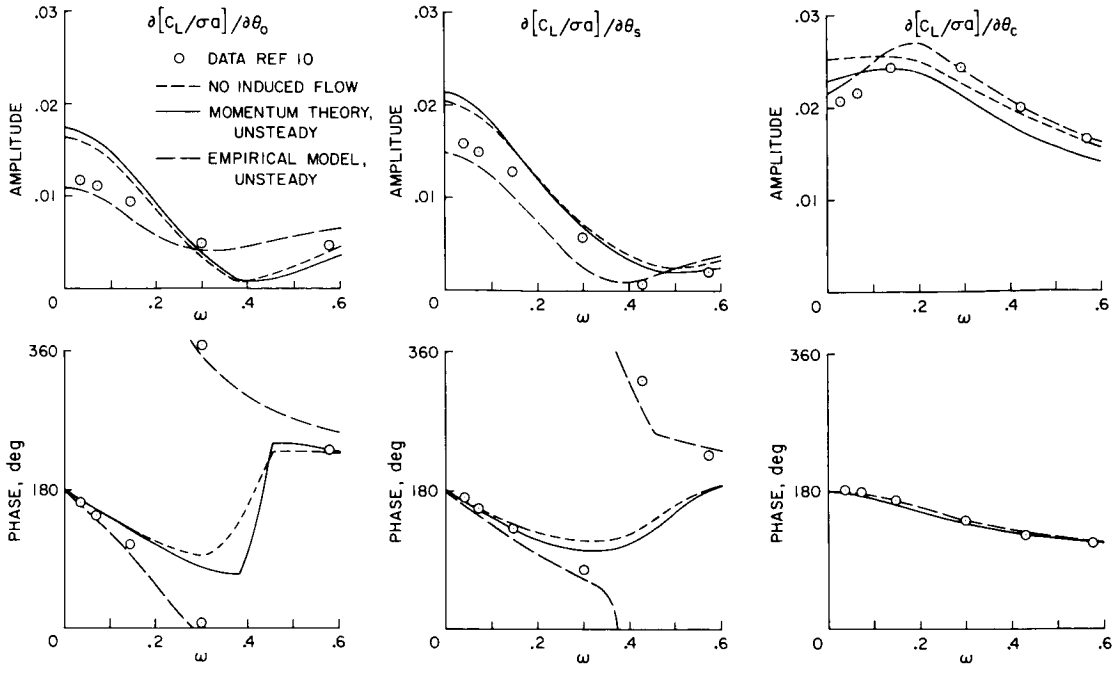

Figure 13. Effect of induced flow model on low frequency, roll response, p = 1.15, γ = 4.25, B = 0.97, e_{pc} = 0.25, μ = 0.51, σa = 0.7294, ν = λ = 0, K_I = 0.1132, K_m = 0.8488, single rotating mode.

References

1. Shupe, N. K., "A Study of the Dynamic Motions of Hingeless Rotored Helicopter," PhD. Thesis, Princeton Univ.

2. Ormiston, R. A. and Peters, D. A., "Hingeless Rotor Response with Nonuniform Inflow and Elastic Blade Bending," Journal of Aircraft, Vol. 9, No. 10, October 1972, pp. 730-736.

3. Hohenemser, K. H. and Yin, Sheng-Kwang, "On the Question of Adequate Hingeless Rotor Modeling in Flight Dynamics," 29th Annual National Forum of the American Helicopter Society, Preprint No. 732, May 1973.

4. Crews, S. T., Hohenemser, K. H., and Ormiston, R. A., "An Unsteady Wake Model for a Hingeless Rotor," Journal of Aircraft, Vol. 10, No. 12, December 1973.

5. Potthast, A. J., "Lockheed Hingeless Rotor Technology Summary - Flight Dynamics", Lockheed Report LR 259871, June 1973, p. 43.

6. Bisplinghoff, R. L., Ashley, H., and Halfman, R. L., Aeroelasticity, Addison-Wesley, Reading, Mass., c. 1955.

7. Peters, D. A. and Hohenemser, K. H., "Application of the Floquet Transition Matrix to Problems of Lifting Rotor Stability," Journal of the American Helicopter Society, Vol. 16, No. 2, April 1971, pp. 25-33.

8. Carpenter, P. J. and Fridovich, B., "Effect of Rapid Blade Pitch Increase on the Thrust and Induced Velocity Response of a Full Scale Helicopter Rotor," NACA TN 3044, Nov. 1953.

9. Tuckerman, L. B., "Inertia Factors of Ellipsoids for Use in Airship Design," NACA Report No. 210, 1925.

10. Ormiston, R. A., "An Actuator Disc Theory for Rotor Wake Induced Velocities," presented at AGARD Specialists' Meeting on the Aerodynamics of Rotary Wings, September 1972.

11. Kuczynski, W. A., "Experimental Hingeless Rotor Characteristics at Full Scale First Flap Mode Frequencies," NASA CR 114519, October 1972.